CMS Physics Analysis Summary

Study of exclusive two-photon production of W^+W^- pairs in pp collisions at 7 TeV, and constraints on anomalous quartic couplings

The CMS Collaboration

Abstract

A search for exclusive or quasi-exclusive W^+W^- production by two-photon exchange, $pp \rightarrow p^{(*)}W^+W^-p^{(*)}$, at $\sqrt{s}$ = 7 TeV is reported using data collected by the CMS detector corresponding to an integrated luminosity of 5.05 fb^{-1}. Events are selected by requiring a $\mu^{\pm}e^{\mp}$ vertex with no associated charged tracks, and dilepton transverse momentum $p_T(\mu^{\pm}e^{\mp}) > 30$ GeV. Two events passing all selection requirements are observed in the data, compared to a Standard Model expectation of 2.2 ± 0.5 signal events with 0.84 ± 0.13 background. The tail of the dilepton transverse momentum distribution, with $p_T(\mu^{\pm}e^{\mp}) > 100$ GeV, is studied for deviations from the Standard Model. No events are observed in this region, and the resulting upper limits are compared to predictions involving anomalous quartic gauge couplings.

1 Introduction

The detection of high-energy photon interactions at the Large Hadron Collider (LHC) opens up the possibility of interesting and novel research [1, 2]. In particular, measurements of the two-photon production of W^+W^- pairs would provide unique sensitivity to anomalous quartic couplings of the gauge bosons. Exploratory studies [3, 4] showed potential for extending the experimental reach by several orders of magnitude with respect to the best limits so far, obtained at LEP [5–12]. First measurements of the exclusive two-photon production of muon and electron pairs at $\sqrt{s} = 7$ TeV, $pp \to p\ell^+\ell^-p$, were made using the 2010 data collected by CMS at the LHC [13, 14]. The present analysis is based on the experimental technique developed in Ref. [13], and uses the full data sample collected by CMS in 2011.

In this analysis the $\ell^+\ell^-$ final state is used to search for fully exclusive ("elastic") $pp \to pW^+W^-p$ production. Since both very forward-scattered protons escape detection, such a production process is characterized by a primary vertex with only a $\ell^+\ell^-$ pair associated to it, as well as by large pair transverse momentum $p_T(\ell^+\ell^-)$ and invariant mass $m(\ell^+\ell^-)$. This signature is also provided by quasi-exclusive ("inelastic" or "proton dissociative") production, where one or both incident protons dissociate into a low mass system that escapes detection, denoted as p^*. The two-photon signal is therefore comprised of both the elastic and inelastic contributions.

In the case of same-flavor decays of the W^+W^- pair, to $\mu^+\mu^-$ or e^+e^- final states, the backgrounds are more than an order of magnitude larger than in the $\mu^\pm e^\mp$ final state. Therefore in the present analysis, only the $\mu^\pm e^\mp$ channel is used to search for a $pp \to p^{(*)}W^+W^-p^{(*)}$ signal. We instead use the $\mu^+\mu^-$ channel to select a control sample of high-mass $pp \to p^{(*)}\mu^+\mu^-p^{(*)}$ events originating mainly from direct $\gamma\gamma \to \mu^+\mu^-$ production. Final states containing a $\mu^\pm e^\mp$ pair may arise from direct decays of W's to electrons and muons, or from $W \to \tau\nu$ decays, with the τ subsequently decaying to an electron or a muon. For brevity, we will refer to the full reaction as $pp \to p^{(*)}W^+W^-p^{(*)} \to p^{(*)}\mu^+e^-p^{(*)}$, where the final state is understood to contain between two and four undetected neutrinos, in addition to the charged $\mu^\pm e^\mp$ pair.

We first use the $pp \to p^{(*)}\mu^+\mu^-p^{(*)}$ control sample to validate the vertexing and exclusivity efficiencies, to verify the pile-up dependence of the selection, and to estimate from the data the quasi-exclusive, inelastic contribution. The dominant backgrounds in the $\mu^\pm e^\mp$ channel, due to the inclusive production of W^+W^- and $\tau^+\tau^-$ pairs, are then constrained using control regions with low $p_T(\mu^\pm e^\mp)$ and/or a low multiplicity of extra tracks on the $\mu^\pm e^\mp$ vertex.

Finally, the data in the signal region is compared to the Standard Model (SM) expectation for the backgrounds and the $\gamma\gamma \to W^+W^-$ signal. The tails of the $p_T(\mu^\pm e^\mp)$ distribution are investigated, where the SM $\gamma\gamma \to W^+W^-$ contribution is expected to be small, to look for anomalous quartic gauge couplings (AQGC) [15].

2 CMS detector

A detailed description of the Compact Muon Solenoid (CMS) experiment can be found elsewhere [16]. The central feature of the CMS apparatus is a superconducting solenoid, of 6 m internal diameter. Within the field volume are the silicon pixel and strip tracker, the crystal electromagnetic calorimeter (ECAL) and the brass-scintillator hadronic calorimeter (HCAL). Muons are measured in gaseous detectors embedded in the iron return yoke. Besides the barrel and endcap detectors, CMS has extensive forward calorimetry.

The CMS detector uses a right-handed coordinate system, with the origin at the nominal collision point, the x-axis pointing to the center of the LHC, the y-axis pointing up (perpendicular

to the LHC plane), and the z-axis along the anticlockwise-beam direction. The polar angle, θ, is measured from the positive z-axis and the azimuthal angle, ϕ, is measured in the (x,y) plane. Based on testbeam results, the ECAL has an energy resolution of better than 0.5% above 100 GeV. The HCAL, when combined with the ECAL, measures jets with a resolution $\Delta E/E \approx 100\%/\sqrt{E} \oplus 5\%$. The calorimeter cells are grouped in projective towers, of granularity $\Delta\eta \times \Delta\phi = 0.087{\times}0.087$ in the region $|\eta| < 1.5$, and increasing to $0.175{\times}0.175$ in the region $3 < |\eta| < 5$. The silicon tracker covers a range of pseudorapidity $|\eta| < 2.4$, and consists of three layers made of 66 million $100{\times}150~\mu\mathrm{m}^2$ pixels followed by ten microstrip layers, with strips of pitch between 80 and 180 $\mu\mathrm{m}$. Muons are measured in the window $|\eta| < 2.4$, with detection planes made of three technologies: Drift Tubes, Cathode Strip Chambers, and Resistive Plate Chambers. Thanks to the strong magnetic field, 3.8 T, and to the high granularity of the silicon tracker, the transverse momentum, p_T, of the muons matched to silicon tracks is measured with a resolution better than ${\sim}1.5\%$, for p_T smaller than 100 GeV. The ECAL provides coverage in a pseudorapidity range of $|\eta| < 1.479$ in a barrel region (EB) and $1.479 < |\eta| < 3.0$ in two endcap regions (EE). The first level (L1) of the CMS trigger system, composed of custom hardware processors, uses information from the calorimeters and muon detectors to select (in less than 1 μs) the most interesting events. The High Level Trigger (HLT) processor farm further decreases the event rate from 100 kHz to a few hundred Hz, before data storage.
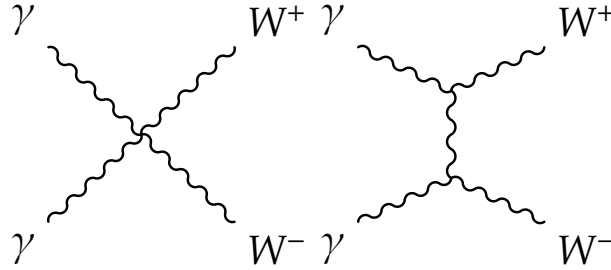
3 Theory and simulation

Figure 1: Quartic and t-channel W exchange diagrams contributing to the $\gamma\gamma \rightarrow W^+W^-$ process at leading order in the SM.

The $\gamma\gamma \rightarrow W^+W^-$ signal is generated using CALCHEP [17], with PYTHIA6 used to decay the W^+W^- pair. The Standard Model process consists of both quartic diagrams and t-channel and u-channel W-exchange (Fig. 1). In models with anomalous triple gauge couplings the quartic $WW\gamma\gamma$ and trilinear $WW\gamma$ interactions can be associated with a single anomalous dimension six operator of the form [15]:

$$L^{WW\gamma} = -ie\frac{\lambda_\gamma}{M_W^2}F^{\mu\nu}W_{\mu\alpha}^\dagger W_\nu^\alpha,$$

where λ_γ has a value of 0 in the SM with no anomalous triple gauge couplings.

The genuine anomalous quartic couplings considered here are instead introduced via an effective Lagrangian containing new terms respecting local $U(1)_{EM}$ and global custodial $SU(2)_C$ symmetry. Further imposing C- and P-symmetry results in a minimum of two additional dimension six terms, containing the parameters a_0^W and a_C^W [15]:

$$L_6^0 = \frac{-e^2}{8}\frac{a_0^W}{\Lambda^2}F_{\mu\nu}F^{\mu\nu}W^{+\alpha}W_\alpha^- - \frac{e^2}{16\cos^2\Theta_W}\frac{a_0^Z}{\Lambda^2}F_{\mu\nu}F^{\mu\nu}Z^\alpha Z_\alpha$$

$$L_6^C = \frac{-e^2}{16} \frac{a_C^W}{\Lambda^2} F_{\mu\alpha} F^{\mu\beta} (W^{+\alpha} W_\beta^- - W^{-\alpha} W_\beta^+) - \frac{e^2}{16 \cos^2 \Theta_W} \frac{a_C^Z}{\Lambda^2} F_{\mu\alpha} F^{\mu\beta} Z^\alpha Z_\beta,$$

where Λ is the scale for new physics. These genuine anomalous quartic couplings are therefore completely independent of the Standard Model triple and quartic couplings.

While the $\gamma\gamma \rightarrow W^+W^-$ process involves two triple gauge coupling vertices involving t-channel W boson exchange (Figure 1), the sensitivity to anomalous triple gauge couplings is not expected to significantly surpass the existing experimental limits on $WW\gamma$ couplings from single TGC processes [4]. Hence, only the genuine anomalous quartic couplings are considered in the present analysis, with no deviation from the Standard Model in the triple gauge couplings assumed.

The existing constraints on the anomalous quartic couplings from e^+e^- collisions at LEP are derived from $e^+e^- \rightarrow W^+W^-\gamma$ and $W^+W^- \rightarrow \gamma\gamma$ interactions, in which the $\gamma\gamma$ center of mass energy is limited to values well below the e^+e^- center of mass energy of $\sqrt{s} = 209$ GeV. In contrast, the spectrum of $\gamma\gamma$ interactions at the the LHC extends to much higher values, resulting in increased sensitivity to the anomalous couplings.

The $\gamma\gamma \rightarrow W^+W^-$ cross section increases quadratically with the anomalous couplings, and consequentely unitarity is violated for high energy $\gamma\gamma$ interactions. For anomalous couplings a_0^W/Λ^2, a_C^W/Λ^2 of order 10^{-5}, the unitarity bound is reached already for collisions with $W_{\gamma\gamma} \sim 1$ TeV [3, 4]. In order to tame this rising of the cross section, both a_0^W/Λ^2 and a_C^W/Λ^2 parameters may be multiplied by a dipole form factor:

$$a_{0,C}^W(W_{\gamma\gamma}^2) = \frac{a_{0,C}^W}{\left(1 + \frac{W_{\gamma\gamma}^2}{\Lambda^2}\right)^p},$$

where $W_{\gamma\gamma}$ is the $\gamma\gamma$ center-of-mass energy, and p is a free parameter, which is conventionally set to 2, following previous studies of AQGCs [18, 19]. Since the energy scale and exact form of the new physics that enters to regulate the cross section is *a priori* unknown, in the current analysis we consider both a scenario with dipole form factors with $\Lambda = 500$ GeV, and a scenario with no form factors.

The simulated inclusive background samples used in this analysis are produced with MAD-GRAPH [20] for W^+W^- + jets, W + jets, and $t\bar{t}$ processes, and PYTHIA6 associated to POWHEG [21–24] for $\tau^+\tau^-$ pairs produced via the Drell-Yan process. The W^+W^- background is scaled to the NLO prediction obtained from MCFM [25], which describes the experimentally measured cross section [26–28] within uncertainties. The diffractive W^+W^- background is generated using POMPYT [29], while the two-photon processes $\gamma\gamma \rightarrow \mu^+\mu^-$ and $\gamma\gamma \rightarrow \tau^+\tau^-$ are produced using LPAIR [30, 31], which describes well the exclusive dilepton measurements of CMS [13, 14]. The contribution from strong central exclusive production of W^+W^- pairs is estimated to be $\leq 1\%$ of the $\gamma\gamma \rightarrow W^+W^-$ cross section, and is neglected in the current analysis [32]. The VBFNLO generator is used to study backgrounds from $WW \rightarrow WW$ scattering [33], with PYTHIA6 used for hadronization and the decay of the W^+W^- pair. All signal and background samples are produced with a detailed GEANT [34] simulation of the CMS detector.

4 Event selection

The data used in this analysis correspond to that collected in 2011 at $\sqrt{s} = 7$ TeV with the CMS detector. In the $\mu^\pm e^\mp$ channel all detector subsystems are required to pass the usual data

quality requirements, resulting in an integrated luminosity of 5.05 fb^{-1}. In the $\mu^+\mu^-$ channel a less restrictive selection is used, requiring that only the muon or tracking systems pass the data quality requirements. This results in a slightly higher integrated luminosity of 5.24 fb^{-1}.

In the $\mu^\pm e^\mp$ channel events are selected by electron-muon triggers with asymmetric 17 GeV and 8 GeV (8 GeV and 17 GeV) thresholds on the electron and muon (muon and electron). For consistency with the $\mu^\pm e^\mp$ channel, dimuon triggers with asymmetric 17 GeV and 8 GeV thresholds on the two muons are used.

Muon candidates are required to pass a tight muon selection, similar to that described in detail in Ref. [13]. Electrons are required to pass a "medium" identification selection, with criteria chosen to ensure the offline selection is tighter than the trigger. The electron selection is similar to that of Ref. [35], and includes requirements on the shower shape measured in the ECAL, the transverse and longitudinal impact parameters, an isolation criterion based on combined information from the silicon tracker and calorimeters, the number of missing hits on the electron track, and the compatibility of the electron and nearby tracks with originating from a photon conversion. For the pair, both $\mu^\pm e^\mp$ and $\mu^+\mu^-$ channels are required to pass the appropriate trigger and to have an invariant mass $m(\ell^+\ell^-) > 20$ GeV. The events are further required to have 15 or less additional tracks associated to the $\ell^+\ell^-$ vertex. The efficiency for lepton reconstruction of primary vertices with two tracks in a cluster has been measured to be approximately 98% in simulation, and almost 99% in data [36].

In the $\mu^\pm e^\mp$ channel, the SM signal region is defined to have zero extra tracks associated to the $\mu^\pm e^\mp$ vertex, and transverse momentum of the pair $p_T(\mu^\pm e^\mp) > 30$ GeV to suppress the backgrounds from $\tau^+\tau^-$ events. In addition, events are only accepted as $\mu^\pm e^\mp$ events if they have failed to satisfy the $\mu^\pm\mu^\mp$ selection, in order to reject $\gamma\gamma \to \mu^+\mu^-$ events with the muon misidentified as an electron.

For the AQGC search, a restricted region of $p_T(\mu^\pm e^\mp) > 100$ GeV is used. This is chosen to reduce the expected SM $\gamma\gamma \to W^+W^-$ contribution to approximately 0.1 events after all selection requirements, while retaining sensitivity to anomalous couplings of order 10^{-4} for $\Lambda = 500$ GeV and larger (Figure 2). This corresponds to values of the AQGC parameters approximately two orders of magnitude smaller than the most stringent limits obtained at LEP [7, 10, 12].

5   Benchmark with $\mu^+\mu^-$ events

In the case of same-flavor dilepton final states, the background to the $\gamma\gamma \to W^+W^-$ signal due to Drell-Yan or direct, exclusive $pp \to p^{(*)}\ell^\pm\ell^\mp p^{(*)}$ production is more than an order of magnitude larger than in the $\mu^\pm e^\mp$ channel. The exclusive $\mu^+\mu^-$ production is used instead as a test benchmark for high mass lepton pair detection, due to the small theoretical uncertainties on the cross section. This sample is then used to validate the efficiency of the vertexing and exclusivity selection, and the dependence on different pile-up conditions.

The dimuon sample with zero extra tracks is divided into two kinematic regions based on the p_T balance ($|\Delta p_T(\mu^+\mu^-)|$) and acoplanarity ($1 - |\Delta\phi(\mu^+\mu^-)/\pi|$) of the pair. The region with $1 - |\Delta\phi(\mu^+\mu^-)/\pi| < 0.1$ and $|\Delta p_T(\mu^+\mu^-)| < 1$ GeV is defined as "elastic" sample, with both protons remaining intact and containing a large fraction of elastic $pp \to p\mu^+\mu^- p$ events. On the other hand, the region with $1 - |\Delta\phi(\mu^+\mu^-)/\pi| > 0.1$, or $|\Delta p_T(\mu^+\mu^-)| > 1$ GeV is dominated by $\gamma\gamma \to \mu^+\mu^-$ interactions in which one or both protons dissociate. As the latter process is less well-known theoretically, and subject to rescattering corrections at high $p_T(\mu^+\mu^-)$ not
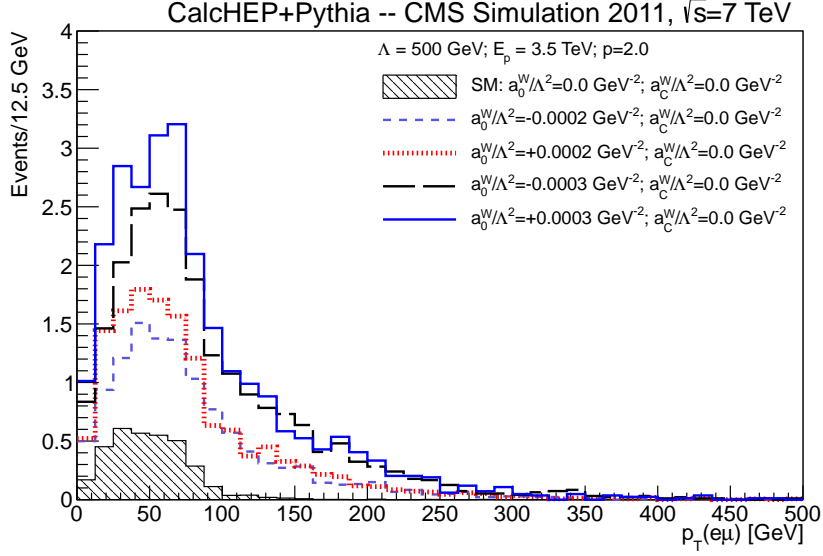
Figure 2: Transverse momentum distribution of lepton pairs for the $\gamma\gamma \rightarrow W^+W^-$ process at generator level in the SM (shaded histogram), and for several values of AQGC parameter a_0^W, while a_C^W is set to zero (open histograms). In this plot $\Lambda = 500$ GeV is the scale for new physics and p is set to 2.0. All distributions are scaled to a integrated luminosity of 5.05 fb^{-1}.

included in the simulation, the second region is used to determine the contribution of proton-dissociation.

The contribution from exclusive Z^0 photoproduction is expected to be smaller than 1 fb after the branching fraction to $\mu^+\mu^-$ [37–39], and the $\gamma\gamma \rightarrow Z$ process is forbidden at tree level. The Z^0 peak therefore provides another cross-check of the residual Drell-Yan contamination in both regions. In Figure 3 the invariant mass distribution after pre-selection is shown, with the marked Z^0 peak region defined as 70 GeV $< m(\mu^+\mu^-) < 106$ GeV. In Figure 4 the dimuon kinematic distributions for events having zero extra tracks are shown. The distributions are plotted separately for the Z^0 peak region, expected to include a large inclusive Drell-Yan component, and for the region outside the Z^0 peak, expected to be dominated by two photon interactions. For the kinematic distributions with zero extra tracks, good agreement is observed between data and simulation. This confirms that event pile-up effects and low multiplicity fluctuations of the inclusive Drell-Yan processes are well modeled. The hatched bands indicate the statistical uncertainty. In Figure 5 the dimuon pair invariant mass is plotted for the dissociation selection with zero extra tracks.

Table 1 lists the number of events with zero extra tracks in data and expected from simulation in the $\mu^+\mu^-$ sample. In the elastic region, the sum of all contributions in simulation is $\sim 10\%$ greater than the yield observed in data. In the dissociation region an overall deficit of 28% is observed in the data. As seen in Figure 6, this deficit is particularly large at high $p_T(\mu^+\mu^-)$ as the process is expected to be increasingly affected by survival probability. As a result the deficit also increases with the invariant mass of the produced pairs.

This suppression is particularly significant in case of quasi-exclusive production when one or both incident protons dissociate and is practically impossible to calculate from first principles as it involves very soft interactions - only phenomenological models are available. Therefore, using our clean sample of muon pairs produced via two-photon interactions we use the data to determine an effective, observed "luminosity" of two-photon interactions at high energies, relevant for W pair production.
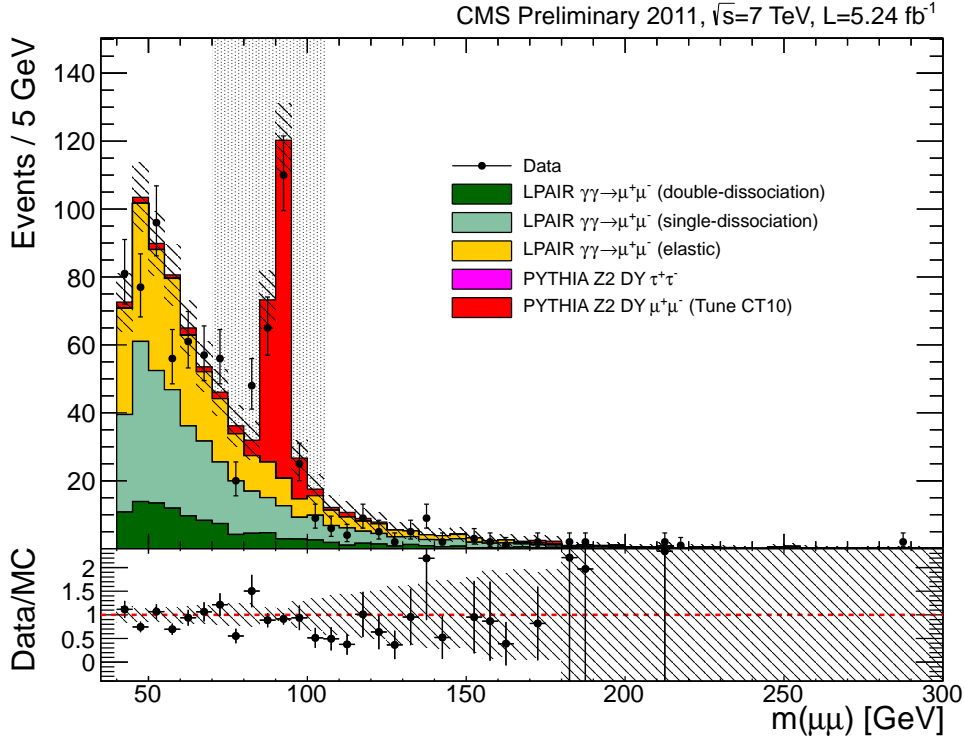
Figure 3: Invariant mass distribution of the muon pairs for the elastic selection. The dotted band indicates the Z^0 peak region. The hatched bands indicate the statistical uncertainty on the simulation.

Region	Data	Simulation	Data/Simulation
Elastic	820 ± 28.6	906.2 ± 30.1	0.905 ± 0.044
Dissociation	1312 ± 36.2	1829.5 ± 42.8	0.717 ± 0.026
Total	2132 ± 46.2	2735.7 ± 52.3	0.779 ± 0.023

Table 1: Review of the total number of data events compared to the sum of all the background events expected in the two control regions.

For this purpose, the number of detected dimuon events with invariant mass over 160 GeV, corrected for the DY contribution, is divided by the prediction for the fully exclusive, elastic production according to LPAIR,

$$F = \frac{N_{\mu\mu\ data} - N_{DY}}{N_{elastic}}\bigg|_{m(\mu^+\mu^-) > 160\ \text{GeV}}$$

A total uncertainty of 20% on this factor is assigned, which has two independent sources. The first source is the statistical uncertainty of 15.5% in the determination of this factor from the high-mass dimuon data. The second source is due to the EPA approximation used, which is checked by comparing the matrix element calculations used in LPAIR with the EPA results for muon pair production above 160 GeV in invariant mass, and is taken conservatively as 5%. With a total of 55 data events selecting two muons reconstructed at an invariant mass over 160 GeV, the quantity F is then

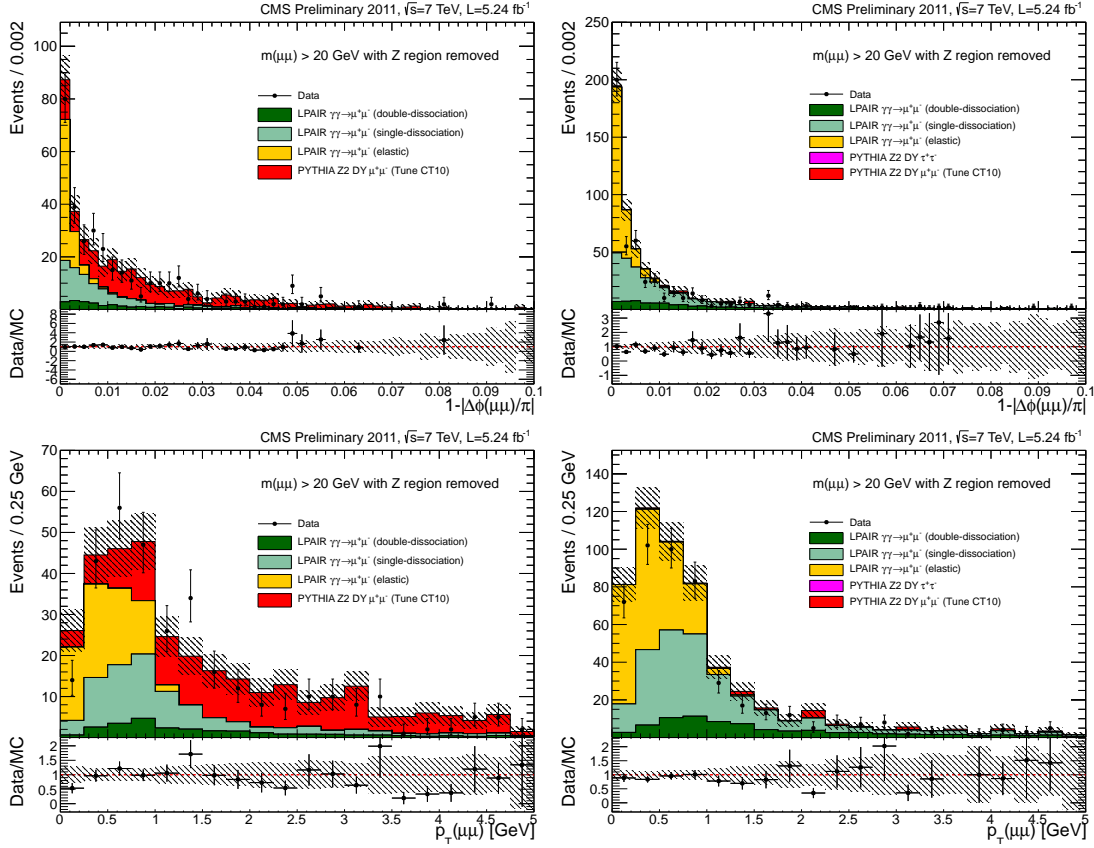$$F = 3.23 \pm 0.50\ (\text{stat.}) \pm 0.36\ (\text{syst.}).$$

Figure 4: Kinematic distributions for the elastic selection, for the Z^0 region only (70 GeV $< m(\mu^+\mu^-) < 106$ GeV, left column) and with the Z^0 region removed (right column). The acoplanarity of $\mu^+\mu^-$ pairs with 0 extra tracks (above), and p_T and Δp_T of $\mu^+\mu^-$ pairs with 0 extra tracks (below) are shown. The hatched bands indicate the statistical uncertainty on the simulation.

This factor F can be then applied, based on the equivalent photon approximation (EPA) [40], to predict the total two-photon production of W pairs. This assumes the dilepton kinematics are the same in fully exclusive and quasi-exclusive production, with the differece in efficiency arising from the requirement of zero extra tracks.

6 WW Signal: the $\mu^\pm e^\mp$ Channel

The SM cross section for the purely elastic process $pp \to pW^+W^-p$ is predicted to be 40.0 fb using CALCHEP, or 0.9 fb for the cross section times branching fraction to $\mu^\pm e^\mp$ final states. Using the scale factor F extracted from the high-mass $\gamma\gamma \to \mu^+\mu^-$ sample to account for the proton dissociation contribution, the total predicted cross section times branching fraction is:

$$\sigma(pp \to p^{(*)}W^+W^-p^{(*)} \to p^{(*)}\mu^\pm e^\mp p^{(*)}) = 3.8 \pm 0.9 \text{ fb}.$$

The acceptance for the SM signal in the fiducial region $|\eta(\mu, e)| < 2.4$, $p_T(\mu, e) > 20$ GeV is 55.1%, taken from the CALCHEP.

In Figure 7, the $p_T(\mu^\pm e^\mp)$ distribution for events passing the preselection and trigger and lepton identification criteria is shown for data and simulation. Table 2 lists the efficiency $\times$ acceptance for the signal at each stage of the selection, the predicted visible cross section, and the corresponding number of events selected in the data.
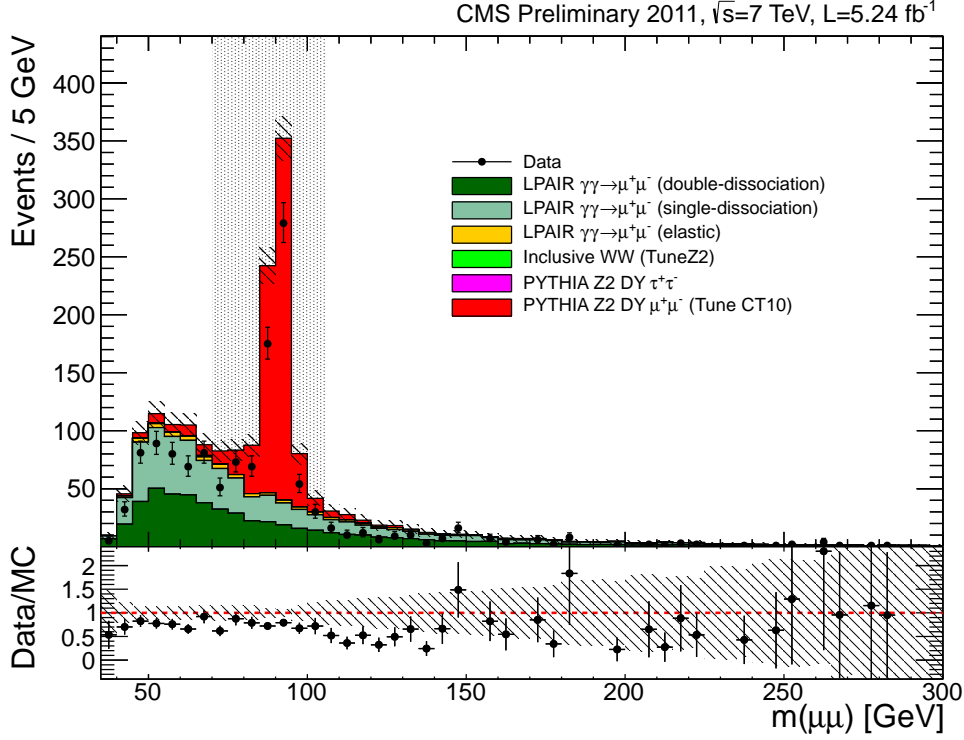
Figure 5: Invariant mass distribution of the muon pairs for the dissociation selection. The dotted band indicates the Z^0 peak region. The hatched bands indicate the statistical uncertainty on the simulation.
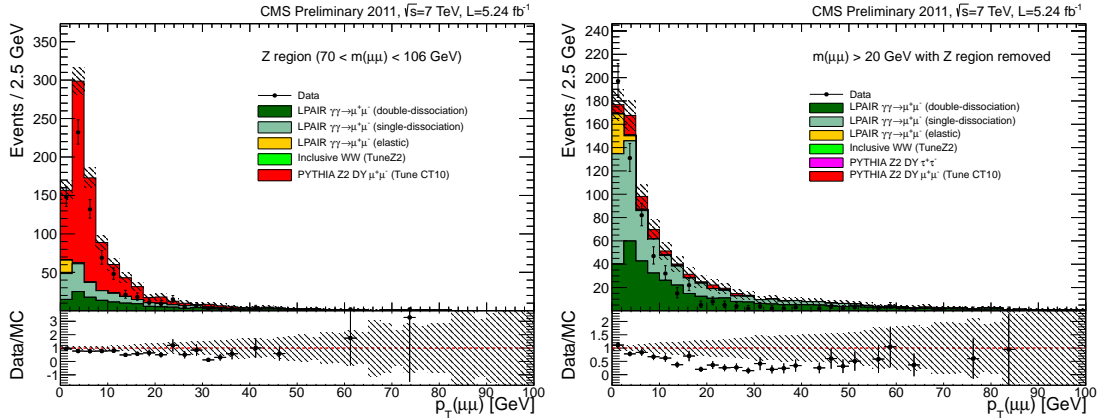

Figure 6: p_T distribution for $\mu^+\mu^-$ pairs with 0 extra tracks passing the dissociation selection, for the Z^0 region only (left), and with the Z^0 region removed (right). The hatched bands indicate the statistical uncertainty on the simulation.

To check the modelling of the individual background contributions, we define orthogonal control regions based on the number of tracks associated to the $\mu^{\pm}e^{\mp}$ vertex, and the p_T of the $\mu^{\pm}e^{\mp}$ pair. To study the inclusive backgrounds, we select control regions with 1-6 extra tracks associated to the $\mu^{\pm}e^{\mp}$ vertex and $p_T(\mu^{\pm}e^{\mp}) < 30$ GeV (dominated by inclusive Drell-Yan $\tau^+\tau^-$), or $p_T(\mu^{\pm}e^{\mp}) > 30$ GeV (dominated by inclusive W^+W^-). In order to select a sample with a significant fraction of exclusive $\gamma\gamma \to \tau^+\tau^-$ events, we define an additional control region having 0 extra tracks, but $p_T(\mu^{\pm}e^{\mp}) < 30$ GeV.

We first compare the data to the expected backgrounds from simulation in the inclusive W^+W^- region. The predicted POMPYT diffractive W^+W^- contribution is, very conservatively, added

Selection step	Signal $\epsilon \times A$	Visible cross section (fb)	Events in data
Trigger and preselection	28.5%	1.4	9086
$m(\mu^\pm e^\mp) > 20$ GeV	28.0%	1.4	8200
Muon ID and Electron ID	22.6%	1.1	1222
$\mu^\pm e^\mp$ vertex with 0 extra tracks	13.7%	0.7	6
$p_T(\mu^\pm e^\mp) > 30$ GeV	10.6%	0.5	2

Table 2: Signal efficiency $\times$ acceptance and number of events selected in data at each stage of the selection. The preselection corresponds to requiring a reconstructed muon and electron of opposite charge, each having $p_T > 15$ GeV and $|\eta| < 2.4$, matched to a common primary vertex with less than 15 additional tracks.
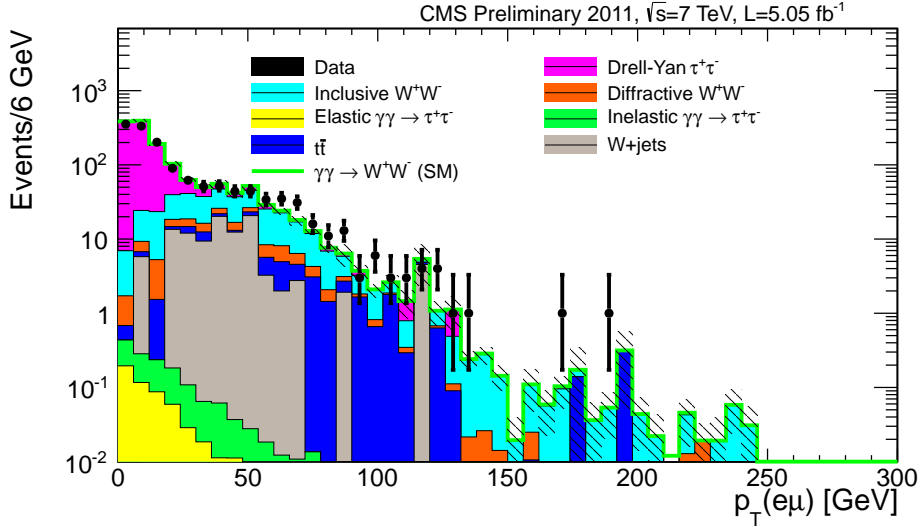
Figure 7: $\mu^\pm e^\mp$ pair transverse momentum. The events plotted are required to pass the trigger and preselection requirements, and the lepton identification. The shaded bands indicate the statistical uncertainty on the background estimation.

to the other backgrounds, without accounting for any survival probabilities or overlap with the inclusive W^+W^- sample. To study the W+jets backgrounds, where the contribution is mainly from fake leptons or non-prompt leptons in jets, we select a control sample of events with $p_T(\mu^\pm e^\mp) > 30$ GeV and at least one of the two leptons failing the nominal offline identification. This sample is then normalized to the simulation in the high-multiplicity (more than 6 extra tracks) region, and used to estimate the W+jets background in the signal and inclusive W^+W^- control regions. Figure 8 shows the distribution of the number of extra tracks for the W^+W^- region with $p_T(\mu^\pm e^\mp) > 30$ GeV. In Figure 9, the invariant mass and acoplanarity of the events with 1-6 extra tracks are plotted. In general the data is consistent with the sum of simulated backgrounds.

The corresponding extra track multiplicity distribution for the Drell-Yan $\tau^+\tau^-$-dominated region with $p_T(\mu^\pm e^\mp) < 30$ GeV is shown in Figure 8. We find a deficit in data compared to simulation in the 1-6 tracks region. In the $\tau^+\tau^-$ sample with zero extra tracks we find 4 events in data, compared to an MC background expectation of 2.5 events, plus 0.9 events of $\gamma\gamma \rightarrow W^+W^-$ signal. The expected contribution to the background from $\gamma\gamma \rightarrow \tau^+\tau^-$ is approximately 0.7 events. The invariant mass and acoplanarity distributions are plotted in Figure 10.

Table 3 summarizes the observed and expected background event yields for the three orthogonal control regions. Due to tracks from pile-up vertices being wrongly associated to the $\mu^\pm e^\mp$
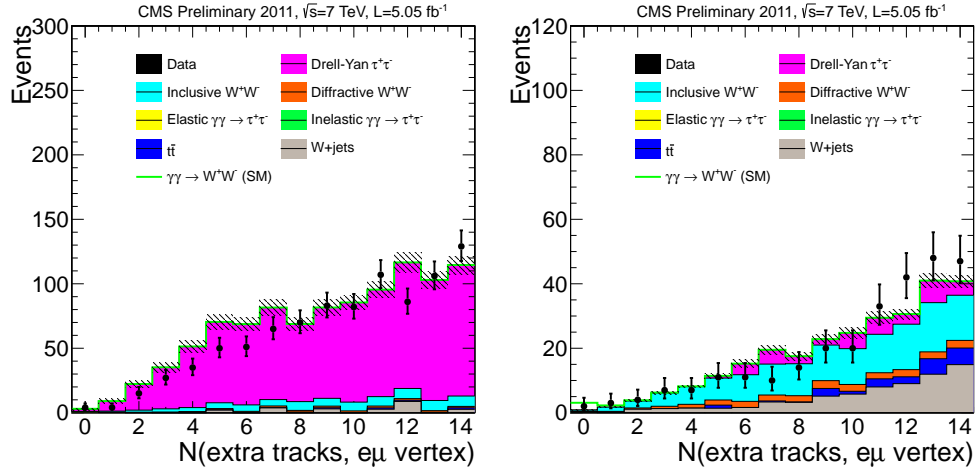
Figure 8: Number of additional tracks on the electron-muon primary vertex and $p_T(\mu^\pm e^\mp) < 30$ GeV (left) and $p_T(\mu^\pm e^\mp) > 30$ GeV (right). The shaded bands indicate the statistical uncertainty on the background estimation.
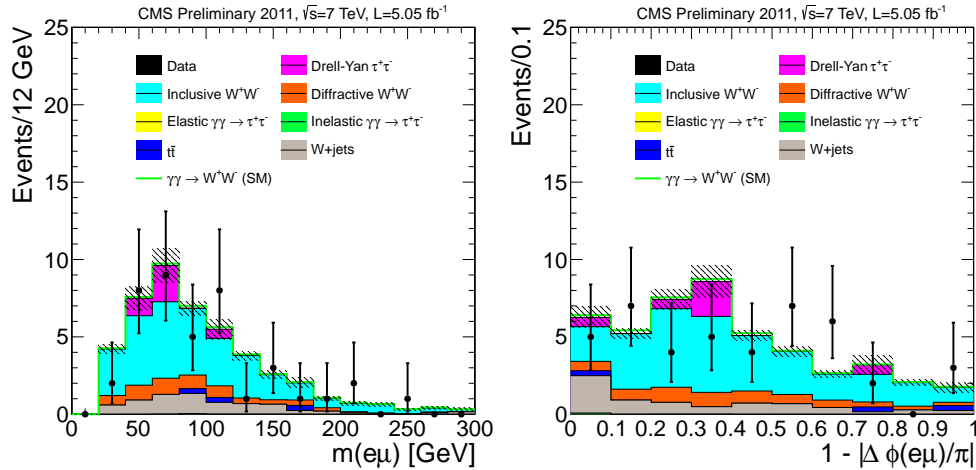

Figure 9: $\mu^\pm e^\mp$ invariant mass (left) and acoplanarity (right) for events with 1-6 extra tracks on the $\mu^\pm e^\mp$ vertex and $p_T(\mu^\pm e^\mp) > 30$ GeV. The shaded bands indicate the statistical uncertainty on the background estimation.

vertex from a $\gamma\gamma \to W^+W^-$ event, signal events may be reconstructed in the 1-6 tracks bins. This signal contamination, as well as that from signal events with $p_T(\mu^\pm e^\mp) < 30$ GeV, is estimated from MC to be approximately 1 event or less in any of the control regions.

We use the simulated background sample, corrected for trigger and lepton identification efficiencies, to estimate the backgrounds in the signal region. The W+jets contribution to the background is estimated from the control sample of events with lepton identification inverted, while the $\gamma\gamma \to \tau^+\tau^-$ is normalized using the factor derived from the high mass $\gamma\gamma \to \mu^+\mu^-$ sample in data. Given the agreement with data in the W^+W^- control region with 1-6 extra tracks, and the $\tau^+\tau^-$ region with zero extra tracks, no additional rescaling of the backgrounds is performed. This results in an estimated background of 0.84 ± 0.13 (stat.) events.

7 Systematics and checks

The systematic uncertainties affecting the signal are summarized in Table 4. The uncertainty on the delivered 2011 luminosity is taken as 2.2% [41]. The lepton trigger and selection efficiency
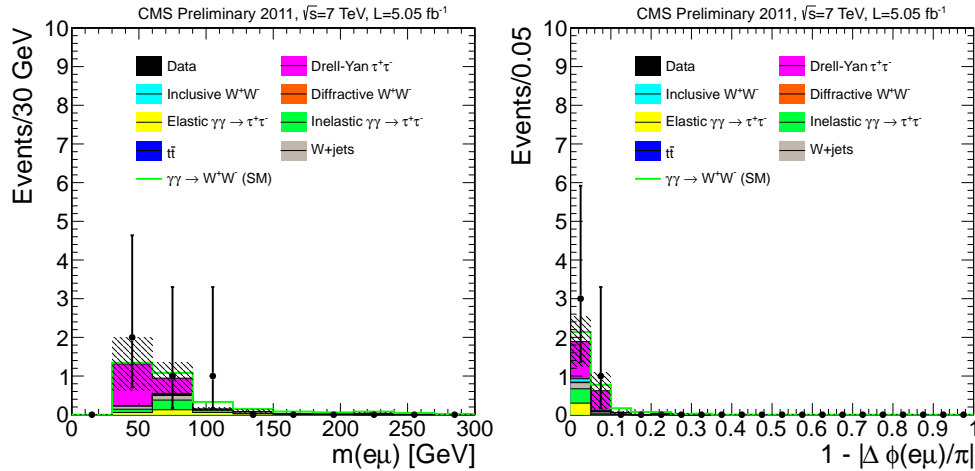
Figure 10: $\mu^{\pm}e^{\mp}$ invariant mass (left) and acoplanarity (right) for events with 0 extra tracks on the $\mu^{\pm}e^{\mp}$ vertex and $p_{\mathrm{T}}(\mu^{\pm}e^{\mp}) < 30$ GeV. The shaded bands indicate the statistical uncertainty on the background estimation.

Region	Data	Sum of MC backgrounds	MC $\gamma\gamma \to W^+W^-$ signal
Inclusive W^+W^-	43	46.2 ± 1.7	1.0
Inclusive Drell-Yan $\tau^+\tau^-$	182	256.7 ± 10.1	0.3
Exclusive $\gamma\gamma \to \tau^+\tau^-$	4	2.6 ± 0.8	0.7

Table 3: Background event yields for the three orthogonal control regions.

corrections are varied by their $\pm 1\sigma$ statistical uncertainties, with the direction of the variation within each p_{T} and η bin correlated. The largest variation in the expected signal (when varying the efficiency scale factors by $+1\sigma$) is 4.2%, which is taken as a systematic uncertainty on the signal yield. The variation in the sum of backgrounds expected from simulation is 3.7%, which is taken as a systematic uncertainty on the background estimate. The uncertainty on the efficiency for reconstructing vertices with two tracks is taken as 1.0%.

The efficiency of the exclusivity selection, including effects from pile-up, is checked using the $\gamma\gamma \to \mu^+\mu^-$ control sample. Using the elastic control region where the theoretical uncertainties are smallest, we assign a 10% systematic uncertainty based on the level of agreement between data and simulation for data samples with lower and higher event pile-up.

The background predictions for both the $\gamma\gamma \to W^+W^-$ signal and the $\gamma\gamma \to \tau^+\tau^-$ background are rescaled to reflect the contribution of proton dissociation, as derived from the high-mass $\gamma\gamma \to \mu^+\mu^-$ sample. A total uncertainty of 20% on the factor F used to take into account the contribution from the inelastic two-photon production is assigned, as described in Section 5. This uncertainty is applied to both the theoretical prediction for the signal, and the $\gamma\gamma \to \tau^+\tau^-$ background prediction.

As a cross-check we perform several alternative estimates and tests of the nominal background contribution of 0.84 ± 0.13 (stat.) events. To check the sensitivity to the Monte Carlo modelling of the dominant W^+W^- background we replace the default MADGRAPH sample with a PYTHIA6 sample, normalized to the NLO cross section. The agreement with data in the control region is similar to MADGRAPH, and results in a total background estimate of 0.71 ± 0.21(stat.) events in the signal region. Scaling the inclusive W^+W^- background to the central value of the CMS cross section measurement [27], rather than the NLO prediction, would change the total background estimate by an amount smaller than the uncertainty on the nominal estimate, to 0.88 ± 0.13 (stat.) events. The sensitivity to the diffractive component of the W^+W^- back-

	Uncertainty
Trigger and lepton identification	4.2%
Luminosity	2.2%
Vertexing efficiency	1.0%
Exclusivity and pile-up dependence	10.0%
Proton dissociation factor	20.0%

Table 4: Summary of systematic uncertainties affecting the signal.

ground is further tested by varying the cross section between 0% and 200% of the nominal value. This results in a variation of ± 0.03 events in the total background estimate. The contribution from vector boson fusion (VBF), $WW \rightarrow WW$, is estimated using the VBFNLO event generator. No VBF events survive all selections, and the contribution in the 1-6 tracks control region is estimated to be approximately 0.1 events.

In addition, we estimate the backgrounds from data using an ABCD method with the three control regions defined in section 6, taking advantage of the lack of correlation between the extra tracks multiplicity and $p_T(\mu^\pm e^\pm) >$ in the main backgrounds. The background in the signal region is obtained from the expression $N_D = (N_A \times N_B)/N_C$, where N_A, N_B, and N_C represent the backgrounds in the inclusive W^+W^-, $\gamma\gamma \rightarrow \tau^+\tau^-$, and inclusive Drell-Yan $\tau^+\tau^-$ control regions, respectively. After subtracting the signal contamination estimated from simulation in each region, the resulting background estimate is 0.77 ± 0.44(stat.) events, with a large statistical uncertainty due to the low statistics in the $\gamma\gamma \rightarrow \tau^+\tau^-$ control region. Performing the same procedure on the simulation as a closure test, we find 0.47 ± 0.15(stat.) events.

We also examine same-sign $\mu^\pm e^\pm$ events in data to check for possible unmodelled backgrounds, since the the main W^+W^- and $\tau^+\tau^-$ backgrounds considered in the analysis are expected to produce opposite-sign lepton pairs. In the 1-6 extra tracks control region we find 8 same sign events with $p_T(\mu^\pm e^\pm) > 30$ GeV passing all selection criteria, and 11 events with $p_T(\mu^\pm e^\pm) < 30$ GeV. No events with fewer than 2 extra tracks on the $\mu^\pm e^\pm$ vertex are observed in the full 2011 data sample.

Finally, we recalculate the $\tau^+\tau^-$ backgrounds using an "embedding" procedure, in which $\mu^+\mu^-$ events are selected in data, and the muons replaced with simulated τ decays to final states containing an electron and a muon [42]. In the Drell-Yan control region with 1-6 extra tracks and $p_T(\mu^\pm e^\pm) < 30$ GeV, for which the largest data vs. simulation discrepency is observed (Table 3), the embedded sample predicts 165.2 ± 3.9 events compared to 182 observed in data. In the signal region, the total background estimated using the embedded sample is 0.67 ± 0.15 events, consistent with the nominal background estimate.

The uncertainty on the background estimate includes the statistical uncertainty of the simulated samples or control samples used to evaluate the backgrounds in the signal region. The uncertainties due to trigger and lepton identification, vertexing efficiency, and the exclusivity selection are also applied to the backgrounds that are taken from simulation. An additional uncertainty of 20% is assigned to the $\gamma\gamma \rightarrow \tau^+\tau^-$ background, reflecting the uncertainty on the normalization of the proton dissociation contribution derived from the $\gamma\gamma \rightarrow \mu^+\mu^-$ control sample.

8 Results

Examining the SM $\gamma\gamma \to W^+W^-$ signal region, we find two events passing all selection criteria, compared to the expectation of 2.2 ± 0.5 signal with 0.84 ± 0.13(stat.) background events.
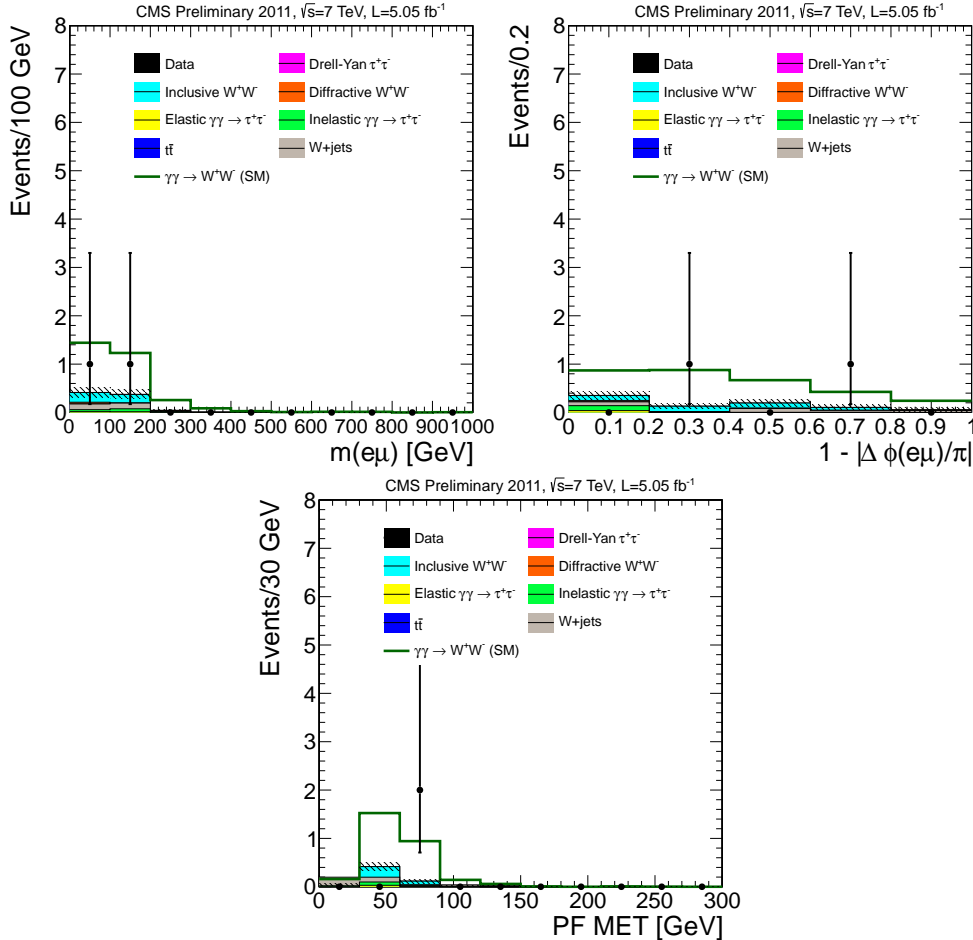

Figure 11: $\mu^\pm e^\mp$ invariant mass (above left), acoplanarity (above right), and missing transverse energy (below) reconstructed with the Particle Flow [43] algorithm, for events in the signal region with 0 extra tracks on the $\mu^\pm e^\mp$ vertex and $p_{\text{T}}(\mu^\pm e^\mp) > 30$ GeV. The backgrounds (solid histograms) are stacked with statistical uncertainties indicated by the shaded region, the signal histogram (open histogram) is stacked on top of the backgrounds.

We convert the observed results into a cross section and upper limit at the proton-proton level, for events with zero extra tracks within $|\eta| < 2.4$. The observed upper limit is estimated using the CL_S method to be $r < 2.2$ times the expected SM yield at 95% CL. The median expected limit in the absence of signal is $r < 1.5^{+1.0}_{-0.6}$. Converting the limit on the number of observed events to a cross section using:

$$\sigma = \frac{N}{\epsilon \times A \times \mathcal{L}},$$

where N is the number of events observed, and $\epsilon \times A$ the efficiency times acceptance for a Standard Model-like signal, we find at 95% CL:

$$\sigma(pp \to p^{(*)}W^+W^-p^{(*)} \to p^{(*)}\mu^\pm e^\mp p^{(*)}) < 8.4 \text{ fb}.$$

Correcting for efficiency, acceptance, and backgrounds, the result interpreted as a cross section times branching fraction is:

$$\sigma(pp \to p^{(*)}W^+W^-p^{(*)} \to p^{(*)}\mu^\pm e^\mp p^{(*)}) = 2.1^{+3.1}_{-1.9} \text{ fb},$$

with a significance of 1.1σ. With statistical uncertainties only, the resulting value of the cross section times branching fraction is $2.1^{+3.0}_{-1.9}(\text{stat.})$ fb. The SM prediction is 3.8 ± 0.9 fb, including the uncertainty on the contribution of proton dissociation.

The $p_T(\mu^\pm e^\mp)$ distribution for events with zero extra tracks is shown in Figure 12. In the AQGC search region $p_T(\mu^\pm e^\mp) > 100$ GeV, zero events are observed in data, consistent with the Standard Model expectation of 0.14, dominated by $pp \to p^{(*)}W^+W^-p^{(*)}$.
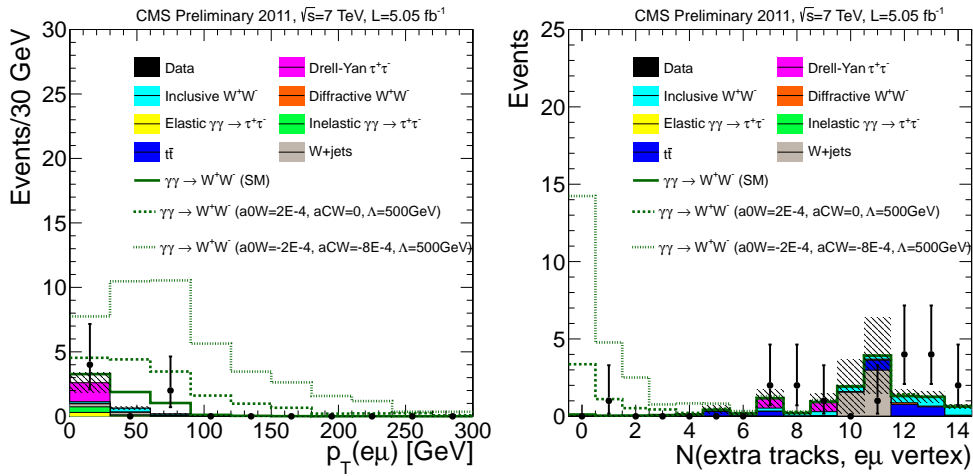
Figure 12: Full $p_T(\mu^\pm e^\mp)$ distribution for events with 0 extra tracks (left) and multiplicity of extra tracks for events with $p_T(\mu^\pm e^\mp) > 100$ GeV (right). The backgrounds (solid histograms) are stacked with statistical uncertainties indicated by the shaded region, the signal histogram (open histogram) is stacked on top of the backgrounds. The expected signal is shown for the SM $\gamma\gamma \to W^+W^-$ signal (solid lines), and for two representative values of the anomalous couplings a_0^W/Λ^2 and a_C^W/Λ^2 (dotted and dashed lines).

We find the selection efficiency does not vary strongly between the SM and AQGC samples tested within the acceptance (Table 5), and therefore set an upper limit on the partial cross section times branching fraction for $\gamma\gamma \to W^+W^- \to \mu^\pm e^\mp$ with $p_T(\mu, e) > 20$ GeV, $|\eta(\mu, e)| < 2.4$, and $p_T(\mu^\pm e^\mp) > 100$ GeV. We treat the residual SM $pp \to p^{(*)}W^+W^-p^{(*)}$ signal as a background, resulting in a total of 0.14 ± 0.02 expected events, and include an additional systematic uncertainty of 10% based on the maximum relative variation of the efficiency between the SM and samples generated with two values of the anomalous couplings.

We find an upper limit of 3 events, corresponding to a 95% CL upper limit on the partial cross section times branching fraction with the selection cuts $p_T(\mu, e) > 20$ GeV, $|\eta(\mu, e)| < 2.4$, and $p_T(\mu^\pm e^\mp) > 100$ GeV:

$$\sigma(pp \to p^{(*)}W^+W^-p^{(*)} \to p^{(*)}\mu^\pm e^\mp p^{(*)}) < 1.9 \text{ fb}.$$

In Figure 13, the excluded value is compared to the predicted cross section for non-zero values of a_0^W/Λ^2 and a_C^W/Λ^2 within the defined acceptance, scaled to include the contribution from proton dissociation. The theoretical prediction is determined from the fully simulated samples,

with one anomalous quartic coupling parameter fixed to zero, and a second order polynomial interpolation of the other. With a dipole form factor of $\Lambda = 500$ GeV, the limits obtained on the AQGC parameters are:

$$-0.00017 < a_0^W/\Lambda^2 < 0.00017 \text{ GeV}^{-2} \ (a_C^W/\Lambda^2 = 0, \Lambda = 500 \text{ GeV}),$$
$$-0.0006 < a_C^W/\Lambda^2 < 0.0006 \text{ GeV}^{-2} \ (a_0^W/\Lambda^2 = 0, \Lambda = 500 \text{ GeV}),$$

which are approximately two orders of magnitude more stringent than the limits obtained at LEP [7, 10, 12].

We perform a similar procedure to scan the two dimensional space of a_0^W/Λ^2 and a_C^W/Λ^2, using a large number of samples generated with a fast simulation of the CMS detector [44]. For each point the cross section and the number of events passing generator selection requirements is used to calculate the observed cross section times branching fraction. This procedure only depends on the generator level prediction, with the fast simulation used to confirm that the signal efficiency of all trigger, reconstruction, and analysis selections, relative to the acceptance is flat across AQGC sample space. The result is shown in Figure 14, where the area outside the ellipse corresponds to values of the anomalous couplings that would result in a partial cross section times branching fraction above 1.9 fb, including the form factor with $\Lambda = 500$ GeV. The result of Ref. [7], obtained from a maximum likelihood fit to a combination of $WW\gamma$ and $WW \rightarrow \gamma\gamma$ channels in e^+e^- collisions, is shown in the inset.

We also obtain the corresponding limits without form factors. In this case the cross section is dominated by the region of high energy $\gamma\gamma$ interactions, above the unitarity bound. This leads to limits on the anomalous couplings much smaller than in the scenario with form factors:

$$-2.80 \times 10^{-6} < a_0^W/\Lambda^2 < 2.80 \times 10^{-6} \text{ GeV}^{-2} \ (a_C^W/\Lambda^2 = 0, \text{no form factor}),$$
$$-1.02 \times 10^{-5} < a_C^W/\Lambda^2 < 1.02 \times 10^{-5} \text{ GeV}^{-2} \ (a_0^W/\Lambda^2 = 0, \text{no form factor}),$$
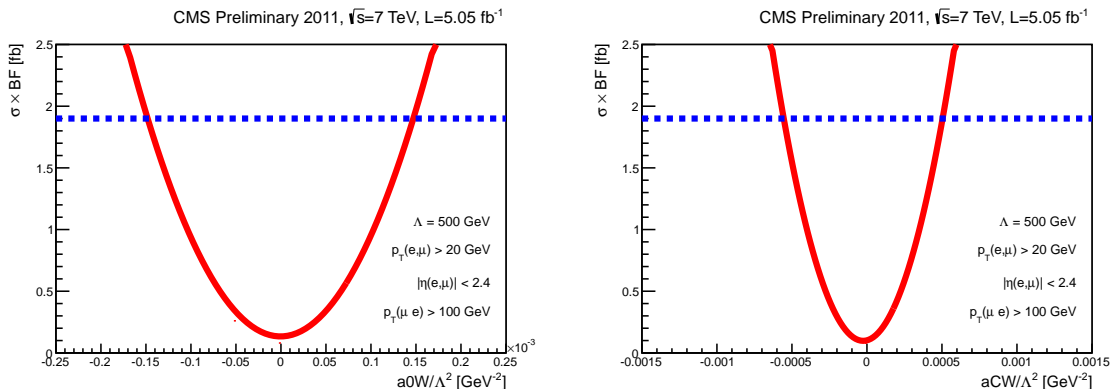
Figure 13: Expected partial cross section times branching fraction with $\Lambda = 500$ GeV as a function of a_0^W/Λ^2 with a_C^W/Λ^2 fixed to 0 (left), and a_C^W/Λ^2 with a_0^W/Λ^2 fixed to 0 (right). The prediction (solid line) and excluded value (dashed line) are both shown for $p_T(\mu, e) > 20$ GeV, $|\eta(\mu, e)| < 2.4$, $p_T(\mu^\pm e^\mp) > 100$ GeV. The prediction is rescaled to include the contribution from proton dissociation.
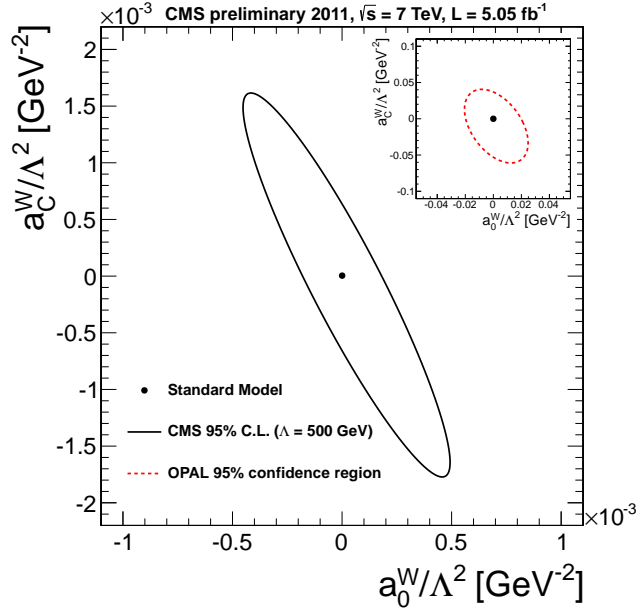
Figure 14: Excluded values of the anomalous coupling parameters a_0^W/Λ^2 and a_C^W/Λ^2 with $\Lambda = 500$ GeV. The area outside the solid line indicates values of the anomalous couplings for which the predicted cross section is above the 95% CL upper limit obtained for $p_T(\mu, e) > 20$ GeV, $|\eta(\mu, e)| < 2.4$, $p_T(\mu^\pm e^\mp) > 100$ GeV. The predicted cross sections are rescaled to include the contribution from proton dissociation. The inset shows the allowed region from the measurement of Ref. [7], obtained from a maximum likelihood fit with the two anomalous couplings as free parameters.

Selection step	SM	Point 1	Point 2	Point 3	Point 4
Efficiency	$30.5 \pm 5.0\%$	$29.8 \pm 2.1\%$	$31.3 \pm 1.8\%$	$36.0 \pm 1.7\%$	$36.3 \pm 1.8\%$

Table 5: Signal efficiency of all trigger, reconstruction, and analysis selections, relative to the acceptance $[p_T(\mu, e) > 20$ GeV, $|\eta(\mu, e)| < 2.4$, $p_T(\mu^\pm e^\mp) > 100$ GeV].

9 Summary

A search for exclusive and quasi-exclusive two-photon production of $W^\pm W^\mp$ in the $\mu^\pm e^\mp$ channel, $pp \to p^{(*)} W^+ W^- p^{(*)} \to p^{(*)} \mu^\pm e^\mp p^{(*)}$, is performed using 5.05 fb^{-1} of data collected at 7 TeV by the CMS detector in 2011. The efficiencies and theoretical predictions for the signal are checked using $\gamma\gamma \to \mu^+ \mu^-$ events, while the backgrounds are constrained from data using control samples in the N(tracks) and $p_T(\mu^\pm e^\mp)$ distributions.

In a region sensitive to SM $\gamma\gamma \to W^+ W^-$ production with $p_T(\mu^\pm e^\mp) > 30$ GeV, 2 events are observed, with a background expectation of 0.84 ± 0.13(stat.). The signal expectation is 2.2 ± 0.5 events, with the uncertainty on the theory reflecting the uncertainty of the proton dissociation contribution. The significance of the signal is 1.1σ, with a 95% CL upper limit on the SM cross section of 8.4 fb.

In the region with $p_T(\mu^\pm e^\mp) > 100$ GeV, where the SM contribution is expected to be small, zero events are observed. A limit is set on the partial cross section times branching fraction within the acceptance of $p_T(\mu, e) > 20$ GeV, $|\eta(\mu, e)| < 2.4$, $p_T(\mu^\pm e^\mp) > 100$ GeV:

$$\sigma(pp \to p^{(*)} W^+ W^- p^{(*)} \to p^{(*)} \mu^\pm e^\mp p^{(*)}) < 1.9 \text{ fb}.$$

We use this subsample to set limits on anomalous quartic coupling parameters, which results

in values on the order of 10^{-4} GeV^{-2} for a_0^W/Λ^2 and 10^{-3} GeV^{-2} for a_C^W/Λ^2, assuming a dipole form factor with $\Lambda = 500$ GeV. These limits are approximately two orders of magnitude more stringent than the best limits obtained at LEP. With no form factors, the limits on the anomalous quartic coupling parameters would be of order 10^{-5} GeV^{-2} and below, driven by high energy $\gamma\gamma$ interactions beyond the unitarity bound. Further improvements in sensitivity could be obtained using the 8 TeV data collected at the LHC during 2012, and by the use of dedicated forward proton detectors [45, 46].

References

[1] D. d'Enterria, M. Klasen, and K. Piotrzkowski, eds., "High-energy photon collisions at the LHC. Proc. Int. Workshop Photon-LHC-2008". *Nucl.Phys.Proc.Suppl.* **179-180**, (2008).

[2] J. de Favereau de Jeneret et al., "High energy photon interactions at the LHC", `arXiv:0908.2020 [hep-ph]`.

[3] T. Pierzchala and K. Piotrzkowski, "Sensitivity to anomalous quartic gauge couplings in photon-photon interactions at the LHC", *Nucl.Phys.Proc.Suppl.* **179-180** (2008) 257–264, `doi:10.1016/j.nuclphysbps.2008.07.032`, `arXiv:0807.1121 [hep-ph]`.

[4] E. Chapon, C. Royon, and O. Kepka, "Anomalous quartic W W gamma gamma, Z Z gamma gamma, and trilinear WW gamma couplings in two-photon processes at high luminosity at the LHC", *Phys.Rev.* **D81** (2010) 074003, `doi:10.1103/PhysRevD.81.074003`, `arXiv:0912.5161 [hep-ph]`.

[5] G. Belanger et al., "Bosonic quartic couplings at LEP-2", *Eur.Phys.J.* **C13** (2000) 283–293, `doi:10.1007/s100520000305`, `arXiv:hep-ph/9908254`.

[6] ALEPH Collaboration Collaboration, "Constraints on anomalous QGC's in e+ e- interactions from 183-GeV to 209-GeV", *Phys.Lett.* **B602** (2004) 31–40, `doi:10.1016/j.physletb.2004.09.041`.

[7] OPAL Collaboration Collaboration, "Constraints on anomalous quartic gauge boson couplings from nu anti-nu gamma gamma and q anti-q gamma gamma events at LEP-2", *Phys.Rev.* **D70** (2004) 032005, `doi:10.1103/PhysRevD.70.032005`, `arXiv:hep-ex/0402021`.

[8] OPAL Collaboration Collaboration, "A Study of $W^+W^-\gamma$ events at LEP", *Phys.Lett.* **B580** (2004) 17–36, `doi:10.1016/j.physletb.2003.10.063`, `arXiv:hep-ex/0309013`.

[9] OPAL Collaboration Collaboration, "Measurement of the $W^+W^-\gamma$ cross-section and first direct limits on anomalous electroweak quartic gauge couplings", *Phys.Lett.* **B471** (1999) 293–307, `doi:10.1016/S0370-2693(99)01357-X`, `arXiv:hep-ex/9910069`.

[10] L3 Collaboration Collaboration, "The $e^+e^- \to Z\gamma\gamma \to q\bar{q}\gamma\gamma$ reaction at LEP and constraints on anomalous quartic gauge boson couplings", *Phys.Lett.* **B540** (2002) 43–51, `doi:10.1016/S0370-2693(02)02127-5`, `arXiv:hep-ex/0206050`.

[11] L3 Collaboration Collaboration, "Study of the $W^+W^-\gamma$ process and limits on anomalous quartic gauge boson couplings at LEP", *Phys.Lett.* **B527** (2002) 29–38, `doi:10.1016/S0370-2693(02)01167-X`, `arXiv:hep-ex/0111029`.

[12] DELPHI Collaboration Collaboration, "Measurement of the $e^+e^- \to W^+W^-\gamma$ cross-section and limits on anomalous quartic gauge couplings with DELPHI", *Eur.Phys.J.* **C31** (2003) 139–147, `doi:10.1140/epjc/s2003-01350-x`, `arXiv:hep-ex/0311004`.

[13] CMS Collaboration Collaboration, "Exclusive photon-photon production of muon pairs in proton-proton collisions at sqrt(s) = 7 TeV", *JHEP* **1201** (2012) 052, `doi:10.1007/JHEP01(2012)052`, `arXiv:1111.5536 [hep-ex]`.

[14] CMS Collaboration Collaboration, "Search for exclusive or semi-exclusive photon pair production and observation of exclusive and semi-exclusive electron pair production in pp collisions at sqrt(s) = 7 TeV", `arXiv:1209.1666 [hep-ex]`.

[15] G. Belanger and F. Boudjema, "Probing quartic couplings of weak bosons through three vectors production at a 500-GeV NLC", *Phys.Lett.* **B288** (1992) 201–209, `doi:10.1016/0370-2693(92)91978-I`.

[16] CMS Collaboration, "The CMS experiment at the CERN LHC", *JINST* **0803** (2008) S08004.

[17] A. Pukhov, "CalcHEP 2.3: MSSM, structure functions, event generation, batchs, and generation of matrix elements for other packages", `arXiv:hep-ph/0412191`.

[18] D0 Collaboration Collaboration, "Studies of WW and WZ production and limits on anomalous $WW\gamma$ and WWZ couplings", *Phys.Rev.* **D60** (1999) 072002, `doi:10.1103/PhysRevD.60.072002`, `arXiv:hep-ex/9905005`.

[19] D0 Collaboration Collaboration, "Limits on anomalous trilinear gauge couplings from $WW \to e^+e^-$, $WW \to e^{\pm}\mu^{\mp}$, and $WW \to \mu^+\mu^-$ events from $p\bar{p}$ collisions at $\sqrt{s} =$ 1.96-TeV", *Phys.Rev.* **D74** (2006) 057101, `doi:10.1103/PhysRevD.74.057101,10.1103/PhysRevD.74.059904`, `arXiv:hep-ex/0608011`.

[20] J. Alwall et al., "MadGraph 5 : Going Beyond", *JHEP* **1106** (2011) 128, `doi:10.1007/JHEP06(2011)128`, `arXiv:1106.0522 [hep-ph]`.

[21] P. Nason, "A New method for combining NLO QCD with shower Monte Carlo algorithms", *JHEP* **0411** (2004) 040, `doi:10.1088/1126-6708/2004/11/040`, `arXiv:hep-ph/0409146`.

[22] S. Frixione, P. Nason, and C. Oleari, "Matching NLO QCD computations with Parton Shower simulations: the POWHEG method", *JHEP* **0711** (2007) 070, `doi:10.1088/1126-6708/2007/11/070`, `arXiv:0709.2092 [hep-ph]`.

[23] S. Alioli et al., "A general framework for implementing NLO calculations in shower Monte Carlo programs: the POWHEG BOX", *JHEP* **1006** (2010) 043, `doi:10.1007/JHEP06(2010)043`, `arXiv:1002.2581 [hep-ph]`.

[24] T. Sjostrand, S. Mrenna, and P. Z. Skands, "PYTHIA 6.4 Physics and Manual", *JHEP* **0605** (2006) 026, `doi:10.1088/1126-6708/2006/05/026`, `arXiv:hep-ph/0603175`.

[25] J. M. Campbell and R. Ellis, "MCFM for the Tevatron and the LHC", *Nucl.Phys.Proc.Suppl.* **205-206** (2010) 10–15, `doi:10.1016/j.nuclphysbps.2010.08.011`, `arXiv:1007.3492 [hep-ph]`.

[26] CMS Collaboration Collaboration, "Measurement of W+W- Production and Search for the Higgs Boson in pp Collisions at sqrt(s) = 7 TeV", *Phys.Lett.* **B699** (2011) 25–47, `doi:10.1016/j.physletb.2011.03.056`, `arXiv:1102.5429 [hep-ex]`.

[27] CMS Collaboration, "Measurement of WW production rate in pp collisions at $\sqrt{s} = 7$ TeV", CMS Physics Analysis Summary CMS-PAS-SMP-12-005, (2012).

[28] ATLAS Collaboration Collaboration, "Measurement of W^+W^- production in pp collisions at $\sqrt{s}$ =7 TeV with the ATLAS detector and limits on anomalous WWZ and WWgamma couplings", `arXiv:1210.2979 [hep-ex]`.

[29] P. Bruni and G. Ingelman, "Diffractive hard scattering at e p and p anti-p colliders", *Conf.Proc.* **C930722** (1993) 595–596.

[30] J. Vermaseren, "Two Photon Processes at Very High-Energies", *Nucl.Phys.* **B229** (1983) 347, `doi:10.1016/0550-3213(83)90336-X`.

[31] S. Baranov et al., "LPAIR: A generator for lepton pair production", in *Hamburg 1991, Proceedings, Physics at HERA, vol. 3* 1478-1482. (see HIGH ENERGY PHYSICS INDEX 30 (1992) No. 12988).* 1991.

[32] P. Lebiedowicz, R. Pasechnik, and A. Szczurek, "Diffractive pQCD mechanism of exclusive production of W^+W^- pairs in proton-proton collisions", *PoS* **QNP2012** (2012) 143, `arXiv:1206.2754`.

[33] K. Arnold et al., "VBFNLO: A Parton Level Monte Carlo for Processes with Electroweak Bosons – Manual for Version 2.5.0", `arXiv:1107.4038 [hep-ph]`.

[34] GEANT4 Collaboration, "GEANT4: A Simulation toolkit", *Nucl.Instrum.Meth.* **A506** (2003) 250–303, `doi:10.1016/S0168-9002(03)01368-8`.

[35] CMS Collaboration Collaboration, "Electron reconstruction and identification at sqrt(s) = 7 TeV",.

[36] "Description and Performance of the CMS Track and Primary Vertex Reconstruction", CMS Note 2011/172, (2011).

[37] V. Goncalves and M. Machado, "Diffractive photoproduction of Z0 bosons in coherent interactions at CERN-LHC", *Eur.Phys.J.* **C56** (2008) 33–38, `doi:10.1140/epjc/s10052-009-1009-z,10.1140/epjc/s10052-008-0633-3`, `arXiv:0710.4287 [hep-ph]`.

[38] L. Motyka and G. Watt, "Exclusive photoproduction at the Tevatron and CERN LHC within the dipole picture", *Phys.Rev.* **D78** (2008) 014023, `doi:10.1103/PhysRevD.78.014023`, `arXiv:0805.2113 [hep-ph]`.

[39] A. Cisek, W. Schafer, and A. Szczurek, "Production of Z0 bosons with rapidity gaps: Exclusive photoproduction in gamma p and pp collisions and inclusive double diffractive Z0's", *Phys.Rev.* **D80** (2009) 074013, `doi:10.1103/PhysRevD.80.074013`, `arXiv:0906.1739 [hep-ph]`.

[40] V. M. Budnev et al., "The two-photon particle production mechanism. Physical problems. Applications. Equivalent photon approximation", *Phys.Rept.* **15** (1975) 181–282, `doi:10.1016/0370-1573(75)90009-5`.

[41] CMS Collaboration, "Absolute Calibration of the Luminosity Measurement at CMS: Winter 2012 Update", CMS Physics Analysis Summary CMS-PAS-SMP-12-008, (2012).

[42] CMS Collaboration Collaboration, "Search for neutral Higgs bosons decaying to τ pairs in pp collisions at $\sqrt{s} = 7$ TeV", *Phys.Lett.* **B713** (2012) 68–90, `doi:10.1016/j.physletb.2012.05.028`, `arXiv:1202.4083`.

[43] CMS Collaboration Collaboration, "Particle-Flow Event Reconstruction in CMS and Performance for Jets, Taus, and MET",.

[44] R. Rahmat, R. Kroeger, and A. Giammanco, "The fast simulation of the CMS experiment", *J.Phys.Conf.Ser.* **396** (2012) 062016, `doi:10.1088/1742-6596/396/6/062016`.

[45] FP420 R&D Collaboration Collaboration, "The FP420 R&D Project: Higgs and New Physics with forward protons at the LHC", *JINST* **4** (2009) T10001, `doi:10.1088/1748-0221/4/10/T10001`, `arXiv:0806.0302 [hep-ex]`.

[46] K. Piotrzkowski, "Tagging two photon production at the CERN LHC", *Phys.Rev.* **D63** (2001) 071502, `doi:10.1103/PhysRevD.63.071502`, `arXiv:hep-ex/0009065`.